

Asymmetric Antibimerons: Statics and Dynamics

Pavel A. Vorobyev,¹ Daichi Kurebayashi,¹ and Oleg A. Tretiakov^{1,*}

¹*School of Physics, The University of New South Wales, Sydney 2052, Australia*

(Dated: October 14, 2024)

The nontrivial topological spin textures, such as magnetic skyrmions, are of great interest due to their potential use as information carriers in spintronic memory and logic. Here, we theoretically predict an asymmetric antibimeron (AAB) – a topological texture in an in-plane magnetized chiral ferromagnet with D_{2d} symmetry, which is yet to be observed experimentally. We show that it can be stabilized by an anisotropic interfacial Dzyaloshinskii-Moriya interaction found in materials with D_{2d} symmetry. Using energy considerations, we explain its asymmetric shape formed of an antivortex and a crescent-shaped vortex of opposite core polarizations. Furthermore, we demonstrate that AABs of opposite topological charge can be stabilized within the same ferromagnetic film, unlike skyrmions in out-of-plane magnetized films. Employing micromagnetic simulations and analytical Thiele's equation approach, we also investigate current-driven dynamics of the AABs, in particular showing that the topological charge of the system can be controllably changed in AAB collisions. Our results shed light on fundamental understanding of asymmetric topological magnetic solitons and provide guidance for their experimental observation in in-plane magnetized ferromagnets.

Introduction.— Over the past few decades, various non-collinear magnetic textures have become the focus of intense research [1, 2]. In the vast majority of recently studied magnetic materials, the stability of these textures results from the Dzyaloshinskii-Moriya interaction (DMI) [3, 4], which is present in crystals with broken inversion symmetry and tries to make magnetic moments perpendicular to each other on neighboring sites. Magnetic skyrmions, which constitute tiny whirls in the magnetic order with nonzero topological charge, serve as a notable example of such textures [5–8]. The topological protection of their magnetic texture, high mobility under spin-polarized currents, and nanometer size hold promise for their applications to ultra-dense information storage [9–11]. The presence or absence of a skyrmion is proposed to encode information bits ‘1’ or ‘0’ [12] for the standard binary logic.

Nevertheless, still substantial challenges remain for memory and logic applications of skyrmions. In particular, ferromagnetic (FM) skyrmions experience transverse deflection from the motion along the current due to the skyrmion Hall effect [13, 14], which may result in their annihilation at the edge of the racetrack. Moreover, the interference between FM skyrmion-based racetracks caused by stray fields impedes higher integration of three-dimensional racetrack devices [15]. One possible way to overcome these challenges in FM materials is to use in-plane counterparts of skyrmions, which are symmetric bimerons [16, 17] shown in Fig. 1(d). While skyrmions and bimerons are topologically equivalent, the latter exhibit different static and dynamic properties [18–25], and in-plane magnetized systems with bimerons produce smaller stray fields.

In this Letter, we propose a model to stabilize a composite texture consisting of an antivortex and crescent-shaped vortex, see Fig. 1(a), which is an in-plane analogue of antiskyrmion [26–28], and therefore dubbed as an asymmetric antibimeron. We demonstrate that the AAB can be stabilized in a chiral ferromagnet with D_{2d} symmetry and investigate its internal structure and current-induced dynam-

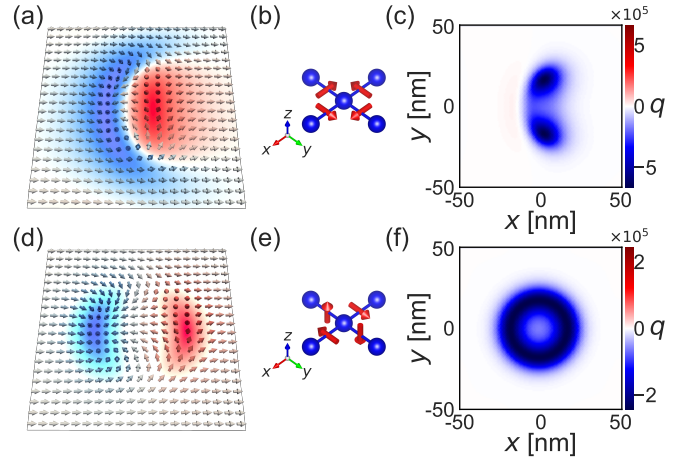


FIG. 1. Asymmetric antibimeron: (a) Magnetic configuration, (b) DMI vectors (red arrows) between neighboring magnetic atoms, and (c) topological charge density. Symmetric bimeron: (d) Magnetic configuration, (e) DMI vectors, and (f) topological charge density.

ics. Moreover, we show that AABs with opposite topological charges can coexist in the same film. Thus, a magnetic system with AABs offers three topologically distinct states, allowing for their clear differentiation, and therefore realizing a prototypical platform for ternary logic [29]. Multi-valued logic systems have recently received significant attention as an approach to develop a more energy-efficient and higher-density electronics [30, 31]. The ternary logic specifically is the most cost-effective when it comes to the use of hardware resources [32, 33]. This logic can be achieved by employing magnetic system with spin textures of three different topological charges. While symmetric bimerons, skyrmions, and antiskyrmions cannot provide this functionality, AABs can. Since these three states are topologically protected, it also reduces the potential for errors. To efficiently operate this logic, we demonstrate that the total topological charge of the system can be tuned in AAB collisions by applying current in different directions.

Model.— We consider a ferromagnetic film with the exchange interaction, uniaxial anisotropy, DMI, and Zeeman coupling. Assuming slowly varying magnetization, the magnetic free energy of the system can be written as

$$F[\mathbf{m}] = \int d^3r \left[A(\nabla \mathbf{m})^2 + \epsilon_a + \epsilon_{\text{DM}} - M_s \mathbf{m} \cdot \mathbf{B} \right], \quad (1)$$

where $A > 0$ is the exchange constant, \mathbf{m} is the normalized magnetization, $\epsilon_a = K_x[1 - (\mathbf{m} \cdot \mathbf{e}_x)^2]$ is the easy-axis anisotropy energy density with anisotropy constant $K_x > 0$, ϵ_{DM} is the DMI energy density, $\mathbf{B} = B_x \mathbf{e}_x$ is the external magnetic field, and M_s is the saturation magnetization. We consider an experimentally relevant DMI found in antiskyrmion systems, such as Heusler compounds $\text{Mn}_{1.4}\text{Pt}_{0.9}\text{Pd}_{0.1}\text{Sn}$ [27] and $\text{Mn}_2\text{Rh}_{0.95}\text{Ir}_{0.05}\text{Sn}$ [34], which takes the form:

$$\epsilon_{\text{DM}} = D(\mathbf{e}_x \cdot \mathbf{m} \times \partial_y \mathbf{m} + \mathbf{e}_y \cdot \mathbf{m} \times \partial_x \mathbf{m}), \quad (2)$$

where D is the DMI constant, and the DMI vectors are depicted in Fig. 1(b) by the red arrows; this type of DMI is allowed under the D_{2d} symmetry. By numerical minimization [35, 36] of the free energy functional, Eq. (1), we obtain an equilibrium magnetic texture shown in Fig. 1(a). This texture is not the ground state, but a lowest excited nontrivial topological state of a system described by free energy F in a certain window of material parameters [37, 38]. AABs are asymmetric spin textures consisting of an antivortex and a crescent-shaped vortex (red and blue regions in Fig. 1(a), respectively). By comparing with a symmetric bimeron [16], shown in Fig. 1(d) and having a different DMI [Fig. 1(e)], where vortex and antivortex have the same arched shape, the antivortex in the AAB is more elliptically symmetric and plays a dominant role as being more energetically favorable for the DMI given by Eq. (2), and thus this texture is called an antitimeron.

To explain the asymmetric shape of the AAB we analyze the influence of the DMI [Eq. (2)] on the spin texture, as among the energy terms in Eq. (1) only the DMI energetically favors out-of-plane spin canting and transforms the uniform magnetic state to a swirling one [39]. This DMI prefers the formation of an antivortex, which has lower energy than the vortex. However, as a single antivortex cannot be stabilized by itself in a uniform in-plane FM background due to the topological constraints, the formation of a vortex with the opposite polarization is required. As a consequence, a coupled pair of vortex and antivortex is formed. Since a symmetric vortex has a higher energy, it is less stable compared to the antivortex and gets deformed to minimize overall energy of the AAB, i.e., vortex wraps around the antivortex in a crescent shape, resulting in an asymmetric shape of the AAB [38].

AABs have interesting topological properties. In general, a nontrivial spin texture is characterized by the topological charge:

$$Q = \int q dx dy, \quad q = \frac{1}{4\pi} \mathbf{m} \cdot \left(\frac{\partial \mathbf{m}}{\partial x} \times \frac{\partial \mathbf{m}}{\partial y} \right), \quad (3)$$

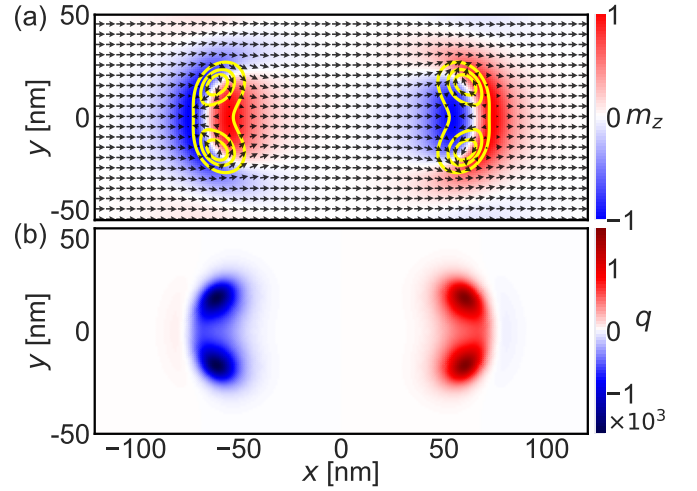


FIG. 2. (a) Magnetization profiles of AABs with opposite topological charges stabilized within the same film. The yellow lines depict contours of topological charge density. The color indicates the magnitude of the m_z . (b) The corresponding topological charge density distribution q .

where q is the topological charge density. As shown in Fig. 1(c), q of the AAB shows an asymmetric distribution consisting of two peaks, which is distinct from the symmetric ring-shaped distribution of skyrmions and symmetric bimerons [see Fig. 1(f)]. Another unique AAB's feature is that the AABs with $Q = \pm 1$ have the same energy, and thus they can be simultaneously formed in the same film, as we demonstrate in Fig. 2. The AABs with the opposite Q are connected by the mirror transformation with respect to yz -plane, $\mathcal{M}_x: \mathcal{M}_x \mathbf{m} = [m_x(-x, y), -m_y(-x, y), -m_z(-x, y)]$. Given that the gradient transforms as $\mathcal{M}_x \nabla = [-\partial_x, \partial_y]$, the DMI in Eq. (2) is symmetric under this mirror transformation. One can check that all other terms in the free energy, Eq. (1), are also symmetric under this transformation, and thus the AABs with opposite topological charges possess the same energy [40]. This is in a sharp contrast to symmetric textures, such as skyrmions, antiskyrmions, and symmetric bimerons, where the background magnetization is perpendicular to all the DMI vectors; for instance, when a skyrmion is stabilized, an antiskyrmion is energetically unstable. The degeneracy between AABs with $Q = \pm 1$ is lifted when a magnetic field perpendicular to all the DMI vectors (i.e., along z -axis) is applied. As this field increases, the energy difference between the AABs of opposite topological charges grows until one of the AABs becomes unstable. Utilizing this property, the total topological charge in the system can be selectively controlled by perpendicular magnetic fields. Having these spin textures with $Q = \pm 1$ within the same material would provide desired functionality for ternary devices, with three logic bits “0” (for no AAB) and “ ± 1 ”, which may be utilized for topological computing [18, 41, 42].

Next, we discuss the formation energy of AABs. Similar to skyrmions, an isolated AAB is an excited state in chiral

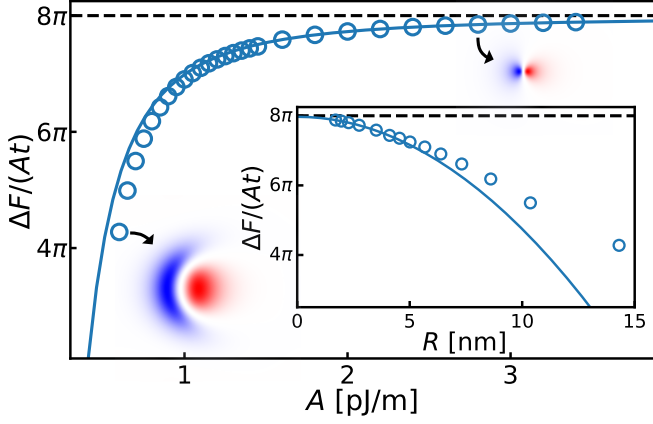


FIG. 3. The formation energy of the AAB, ΔF , as a function of the exchange constant A . The inset shows the relationship between the AAB's energy and its characteristic size R . Blue circles represent numerical data, while blue curves represent the corresponding fittings.

in-plane magnets. As shown in Fig. 3, the formation energy of the AAB with respect to the ground (uniformly magnetized) state asymptotically approaches the Belavin-Polyakov exchange limit [43–45], $\Delta F \rightarrow 8\pi At$, with t being the film thickness, when exchange constant A increases. This is because the increase of A (with all other parameters being fixed) results in smaller AABs with larger rotational angles between neighboring magnetic moments. As the exchange energy is proportional to the square of magnetization gradient, while the other energy terms have weaker dependencies on the spatial magnetization gradients, its contribution becomes dominant in the limit of small AABs. The next correction to the AAB formation energy after the exchange comes from the DMI in a small AAB limit, as it is linear in the gradient of magnetization. We numerically checked that, as the AAB size increases, the DMI gives a negative contribution to the AAB formation energy ΔF . The inset shows ΔF dependence on AAB's characteristic size R . Due to an asymmetric shape of AAB, we define this size as $R = \sqrt{S}$, where S is the area enclosed by $m_x = 0$ contour. Using the relationship between R and A [38], one can deduce from the inset of Fig. 3 that the AAB's formation energy depends approximately linear on R for small AABs. The detailed effect of other energy terms on the AAB size is described in the Supplemental Material [38].

Current-driven motion of AABs.— To study the current-driven dynamics of AABs, we employ the Landau-Lifshitz-Gilbert (LLG) equation describing magnetization evolution under the influence of the spin-transfer torques [46, 47],

$$\frac{d\mathbf{m}}{dt} = \gamma \mathbf{H}_{\text{eff}} \times \mathbf{m} + \alpha \mathbf{m} \times \frac{d\mathbf{m}}{dt} - (\mathbf{u} \cdot \nabla) \mathbf{m} + \beta \mathbf{m} \times (\mathbf{u} \cdot \nabla) \mathbf{m}, \quad (4)$$

where $\mathbf{H}_{\text{eff}} = -(\mu_0 M_s)^{-1} \delta F[\mathbf{m}] / \delta \mathbf{m}$ is the effective magnetic field, μ_0 is the vacuum permeability, $\gamma = g\mu_B / (2mc)$ is the gyromagnetic ratio, α is the Gilbert damping constant, β is the nonadiabatic spin-transfer torque constant, and $\mathbf{u} = P g \mu_B \mathbf{j}_e / (2e M_s)$ with P being the electron's spin polariza-

tion, g being the g -factor, μ_B being the Bohr magneton, and \mathbf{j}_e being the current density.

We numerically solve the LLG equation with the current applied along x -direction ($\mathbf{u} = u_x \mathbf{e}_x$) to analyze the AAB motion. As shown in Fig. 4 (a) and (b), the spin-transfer torque induces not only the translational motion but also the deformation of the texture; the deformation trends depend on the α to β ratio [48]. When $\alpha > \beta$, the AAB shows elongation in the transverse direction and the counterclockwise tilt in addition to the transverse motion with negative transverse velocity, as shown in Fig. 4 (a). The dashed lines are the trajectories of the two peaks of the AAB's topological charge density, shown as two red dots in Fig. 4 (c). On the other hand, when $\alpha < \beta$, the AAB shrinks during the motion, exhibiting a positive AAB Hall angle, as shown in Fig. 4 (b). In this case, the distance between the two peaks, d , see Fig. 4 (c), oscillates in time, indicating repulsive interaction when d becomes small. Note that the AAB Hall angle is proportional to $(\alpha - \beta)$, which explains the sign change for the transverse motion. For $\alpha = \beta$, the system becomes translationally invariant, and thus the AABs move without any deformations.

Figure 4 (d) shows the AAB size after an application of 1 ns pulse for various current strength u_x . The AAB's size linearly increases from its equilibrium size for $\alpha > \beta$. This linear dependence on the applied current suggests that the attractive interaction between two merons, corresponding to two peaks of q , is relatively weak when the distance d is larger than the equilibrium distance. In contrast, for $\alpha < \beta$, the size of the AAB linearly decreases when the applied current is small ($u_x < 100$ m/s), but saturates for larger current due to the repulsive interaction between the two merons [49]. Note that the dependence on $\alpha - \beta$ is inverted, when the applied current direction is reversed. That is, when the current is applied in $-x$ direction, the AAB decreases in size for $\alpha > \beta$, while it elongates for $\alpha < \beta$ [50].

In order to understand this AAB asymmetric dynamics, we employ the generalized Thiele's equation approach [51–53]. When the motion of magnetic textures is described by translation without any deformations, $\mathbf{m}(\mathbf{r}, t) = \mathbf{m}(\mathbf{r} - \mathbf{v}t)$, the center-of-mass dynamics obeys the Thiele's equation, $\hat{G}_{ij}(u_x \mathbf{e}_x - \mathbf{v})_j + \hat{D}_{ij}(\beta u_x \mathbf{e}_x - \alpha \mathbf{v})_j = 0$, where \mathbf{v} is the velocity of the texture, $\hat{G}_{ij} = \int dxdy \mathbf{m} \cdot (\partial_i \mathbf{m} \times \partial_j \mathbf{m})$ is the gyrotropic tensor, and $\hat{D}_{ij} = \int dxdy \partial_i \mathbf{m} \cdot \partial_j \mathbf{m}$ is the dissipative tensor. The subscript indices run over the two-dimensional spatial coordinates, x and y . Obviously, Thiele's approach cannot perfectly describe the AAB dynamics as the texture deforms during the motion. However, if we focus separately on the dynamics of two individual merons, building blocks of the AAB, the motion can be approximated by their simple translation. These two merons are concentrated around the two peaks of topological density in the AAB, see e.g. Fig. 4 (c). As seen from the topological charge density shown in Fig. 1 (c), each meron is elliptically deformed, rotated by approximately $\pm 45^\circ$, and possesses the topological charge of $|Q| = 1/2$. In sharp contrast to symmetric spin textures (e.g., skyrmions or

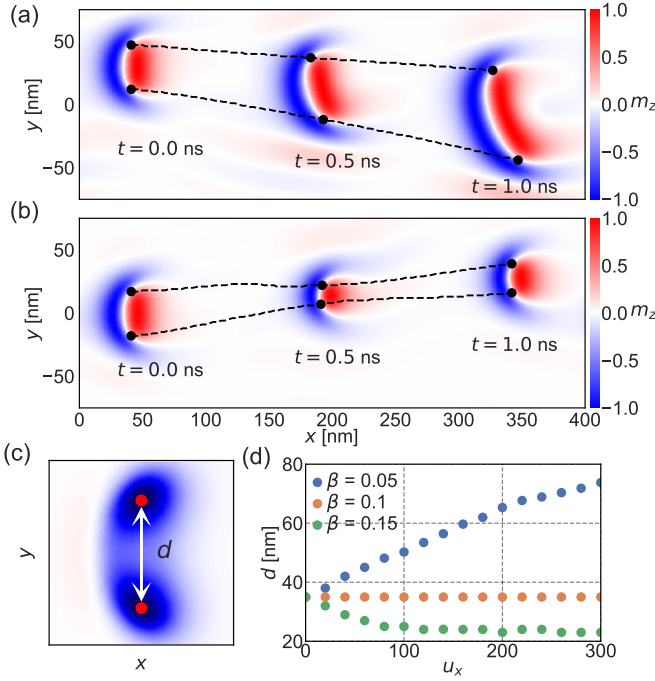


FIG. 4. (a, b) The AAB trajectory under DC current along x -axis for $u_x = 200$, $\alpha = 0.1$ in case of (a) $\beta = 0.05$ and (b) $\beta = 0.15$. The dashed lines are the trajectories of the two peaks of topological charge density. Color indicates the z -component of magnetization. (c) Topological charge density. The characteristic texture size d is defined as the distance between two peaks of the topological charge density indicated by the red dots. (d) The size d after 1 ns current pulse as a function of current strength u_x for $\beta > \alpha$, $\beta = \alpha$, and $\beta < \alpha$ (here $\alpha = 0.1$).

symmetric bimerons), whose \hat{D} is diagonal, the off-diagonal components of the dissipative tensor, D_{xy} , are finite for elliptically deformed merons in the AAB. Importantly, D_{xy} is proportional to $\sin 2\delta$, where δ is the rotation angle of the ellipse. Namely, two merons in an AAB have opposite signs of D_{xy} [54]. Then, the solution of Thiele's equation is obtained as

$$v_x = \frac{Q^2 + \alpha\beta(D^2 - D_{xy}^2) + (\alpha - \beta)QD_{xy}}{Q^2 + \alpha^2(D^2 - D_{xy}^2)}u_x, \quad (5)$$

$$v_y = \frac{(\alpha - \beta)DQ}{Q^2 + \alpha^2(D^2 - D_{xy}^2)}u_x, \quad (6)$$

where v_x and v_y are the longitudinal and transverse velocities of a meron, respectively, and D is the diagonal component of the dissipative tensor. Equation (5) demonstrates that the two merons in an AAB have different longitudinal velocities due to the finite D_{xy} , resulting in elongation and rotation of the texture. Furthermore, the longitudinal velocity [Eq. (6)] is proportional to $(\alpha - \beta)u_x$, indicating the sign change depending on the α/β ratio, which is in excellent agreement with our numerical results [55].

AAB collisions.— Since AABs with opposite topological charges can be simultaneously stabilized in the same film, it

is interesting to consider their collisions. To study these collisions numerically, we drive AABs by current utilizing the spin-transfer torques [Eq. (4)] and use the fact that transverse to the current direction of the AAB motion depends on the sign of Q (due to the antibimeron Hall effect), as shown by Eq. (6). By appropriately arranging the initial positions of AABs, we can move them toward each other.

Firstly, we examine collisions between the AABs of opposite charge by applying the current along y -axis [56]. From the viewpoint of topological charge conservation, a pair annihilation is expected upon the collision. In this case, the size of AABs with opposite Q remains the same during the current-driven motion. As a result, AABs annihilate with each other, thus conserving total topological charge as expected, while the energy released in the collision is carried away by the spin waves. Moreover, we found a critical behavior in this type of collisions. When the applied current is small, the two AABs do not annihilate but just move next to each other along the current [57]. This is due to a repulsive force between AABs associated with their rigidity. On the other hand, in the collisions with the current applied along x -direction [58], the size of AABs changes differently during the motion as discussed above; i.e., one AAB increases in size while the other shrinks, depending on the applied current direction and α/β ratio. Since the smaller AAB is less stable, c.f. Fig. 3, contrary to the previous case, the larger AAB always survives after the collision. Thus, we conclude that the topological charge is not necessarily conserved in AAB collisions. This allows for a change in the overall topological charge in the film with multiple AABs. Therefore, the total Q of the AAB system can be electrically manipulated by applying current in different directions.

Conclusions.— We theoretically propose a model to stabilize asymmetric antibimerons, composite spin textures consisting of antivortex and crescent-shaped vortex, and study their equilibrium and dynamical properties. We show that the AABs can be stabilized in a ferromagnet with an in-plane uniaxial anisotropy and D_{2d} -symmetric DMI. As some Heusler compounds are known to host such DMI [27, 34], we expect that AABs will be experimentally observed in the near future. Moreover, we demonstrate the coexistence of AABs with opposite topological charges in the same film, which is rather distinct from skyrmionic systems, where the sign of the topological charge is uniquely determined. Furthermore, we show that the current-induced dynamics of AABs exhibit anisotropic behavior and depend on the applied current direction, which is explained based on the generalized Thiele's equation. We also demonstrate that the total topological charge in systems with AABs can be changed by static magnetic fields perpendicular to the film's plane or independently via the AAB collisions by selectively applying electric current along or perpendicular to the magnetic anisotropy direction. Ultimately, AABs offer a potential solution for the future realization of spintronic ternary memory and logic. Finally, we note that our results for AABs are fully applicable to other asymmetric spin textures stabilized by different types of

DMIs, such as asymmetric bimerons [19, 59–62] and asymmetric (anti-)skyrmions.

Acknowledgments.—O.A.T. acknowledges the support from the Australian Research Council (Grant Nos. DP200101027 and DP240101062) and the NCMAS grant.

P.A.V. and D.K. contributed equally to this work. O.A.T. conceived and supervised the project. P.A.V. and D.K. conducted simulations on the static properties. D.K. conducted simulations on the dynamical properties and constructed the analytical theory. All authors contributed to discussions and writing the manuscript.

* o.tretiakov@unsw.edu.au

- [1] A. Kosevich, B. Ivanov, and A. Kovalev, Magnetic solitons, *Phys. Rep.* **194**, 117 (1990).
- [2] B. Göbel, I. Mertig, and O. A. Tretiakov, Beyond skyrmions: Review and perspectives of alternative magnetic quasiparticles, *Phys. Rep.* **895**, 1 (2021).
- [3] I. Dzyaloshinsky, A thermodynamic theory of “weak” ferromagnetism of antiferromagnetics, *J. Phys. Chem. Solids* **4**, 241 (1958).
- [4] T. Moriya, Anisotropic superexchange interaction and weak ferromagnetism, *Phys. Rev.* **120**, 91 (1960).
- [5] A. N. Bogdanov and D. A. Yablonskii, Thermodynamically stable “vortices” in magnetically ordered crystals. the mixed state of magnets, *Sov. Phys. JETP* **68**, 101 (1989).
- [6] U. K. Röbber, A. N. Bogdanov, and C. Pfleiderer, Spontaneous skyrmion ground states in magnetic metals, *Nature* **442**, 797 (2006).
- [7] N. Nagaosa and Y. Tokura, Topological properties and dynamics of magnetic skyrmions, *Nat. Nanotechnol.* **8**, 899 (2013).
- [8] S. Mühlbauer, B. Binz, F. Jonietz, C. Pfleiderer, A. Rosch, A. Neubauer, and R. G. P. Boni, Skyrmion lattice in a chiral magnet, *Science* **323**, 915 (2009).
- [9] N. Romming, C. Hanneken, M. Menzel, J. E. Bickel, B. Wolter, K. von Bergmann, A. Kubetzka, and R. Wiesendanger, Writing and deleting single magnetic skyrmions, *Science* **341**, 636 (2013).
- [10] N. S. Kiselev, A. N. Bogdanov, R. Schäfer, and U. K. Röbber, Chiral skyrmions in thin magnetic films: new objects for magnetic storage technologies?, *J. Phys. D: Appl. Phys.* **44**, 392001 (2011).
- [11] J. Sampaio, V. Cros, S. Rohart, A. Thiaville, and A. Fert, Nucleation, stability and current-induced motion of isolated magnetic skyrmions in nanostructures, *Nat. Nanotechnol.* **8**, 839 (2013).
- [12] A. Fert, V. Cros, and J. Sampaio, Skyrmions on the track, *Nat. Nanotechnol.* **8**, 152 (2013).
- [13] K. Litzius, I. Lemesh, B. Krüger, P. Bassirian, L. Caretta, K. Richter, F. Büttner, K. Sato, O. A. Tretiakov, J. Förster, R. M. Reeve, M. Weigand, I. Bykova, H. Stoll, G. Schütz, G. S. D. Beach, and M. Kläui, Skyrmion hall effect revealed by direct time-resolved x-ray microscopy, *Nat. Phys.* **13**, 170 (2017).
- [14] W. Jiang, X. Zhang, G. Yu, W. Zhang, X. Wang, M. Benjamin Jungfleisch, J. Pearson, X. Cheng, O. Heinonen, K. L. Wang, Y. Zhou, A. Hoffmann, and S. G. E. te Velthuis, Direct observation of the skyrmion hall effect, *Nat. Phys.* **13**, 162 (2017).
- [15] K. Gu, Y. Guan, B. K. Hazra, H. Deniz, A. Migliorini, W. Zhang, and S. S. P. Parkin, Three-dimensional racetrack memory devices designed from freestanding magnetic heterostructures, *Nat. Nanotech.* **17**, 1065 (2022).
- [16] B. Göbel, A. Mook, J. Henk, I. Mertig, and O. A. Tretiakov, Magnetic bimerons as skyrmion analogues in in-plane magnets, *Phys. Rev. B* **99**, 060407 (2019).
- [17] Y. A. Kharkov, O. P. Sushkov, and M. Mostovoy, Bound states of skyrmions and merons near the Lifshitz point, *Phys. Rev. Lett.* **119**, 207201 (2017).
- [18] X. Li, L. Shen, Y. Bai, J. Wang, X. Zhang, M. E. J. Xia, O. A. Tretiakov, X. Xu, M. Mruczkiewicz, M. Krawczyk, Y. Xu, R. F. L. Evans, R. W. Chantrell, and Y. Zhou, Bimeron clusters in chiral antiferromagnets, *npj Comput. Mater.* **6**, 169 (2020).
- [19] L. Shen, X. Li, J. Xia, L. Qiu, X. Zhang, O. A. Tretiakov, M. Ezawa, and Y. Zhou, Dynamics of ferromagnetic bimerons driven by spin currents and magnetic fields, *Phys. Rev. B* **102**, 104427 (2020).
- [20] H. Jani, J.-C. Lin, J. Chen, J. Harrison, F. Maccherozzi, J. Schäd, S. Prakash, C.-B. Eom, A. Ariando, T. Venkatesan, and P. G. Radaelli, Antiferromagnetic half-skyrmions and bimerons at room temperature, *Nature* **590**, 74 (2021).
- [21] O. J. Amin, S. F. Poole, S. Reimers, L. X. Barton, A. Dal Din, F. Maccherozzi, S. S. Dhesi, V. Novák, F. Krizek, J. S. Chauhan, R. P. Campion, A. W. Rushforth, T. Jungwirth, O. A. Tretiakov, K. W. Edmonds, and P. Wadley, Antiferromagnetic half-skyrmions electrically generated and controlled at room temperature, *Nat. Nanotechnol.* **18**, 849 (2023).
- [22] A. O. Leonov and I. Kézsmárki, Asymmetric isolated skyrmions in polar magnets with easy-plane anisotropy, *Phys. Rev. B* **96**, 014423 (2017).
- [23] L. Shen, J. Xia, X. Zhang, M. Ezawa, O. A. Tretiakov, X. Liu, G. Zhao, and Y. Zhou, Current-induced dynamics and chaos of antiferromagnetic bimerons, *Phys. Rev. Lett.* **124**, 037202 (2020).
- [24] C. Jin, S. Li, H. Zhang, R. Wang, J. Wang, R. Lian, P. Gong, and X. Shi, Spin-wave modes of magnetic bimerons in nanodots, *New J. Phys.* **24**, 073013 (2022).
- [25] N. Gao, S.-G. Je, M.-Y. Im, J. W. Choi, M. Yang, Q. Li, T. Y. Wang, S. Lee, H.-S. Han, K.-S. Lee, W. Chao, C. Hwang, J. Li, and Z. Q. Qiu, Creation and annihilation of topological meron pairs in in-plane magnetized films, *Nat. Commun.* **10**, 5603 (2019).
- [26] W. Koshibae and N. Nagaosa, Theory of antiskyrmions in magnets, *Nat. Commun.* **7**, 10542 (2016).
- [27] A. K. Nayak, V. Kumar, T. Ma, P. Werner, E. Pippel, R. Sahoo, F. Damay, U. K. Röbber, C. Felser, and S. S. P. Parkin, Magnetic antiskyrmions above room temperature in tetragonal heusler materials, *Nature* **548**, 561 (2017).
- [28] M. N. Potkina, I. S. Lobanov, O. A. Tretiakov, H. Jónsson, and V. M. Uzdin, Stability of long-lived antiskyrmions in the Mn-Pt-Sn tetragonal Heusler material, *Phys. Rev. B* **102**, 134430 (2020).
- [29] See Supplemental Material at [URL will be inserted by publisher] for more details on ternary logic.
- [30] M. Andreev, S. Seo, K.-S. Jung, and J.-H. Park, Looking beyond 0 and 1: Principles and technology of multi-valued logic devices, *Adv. Mater.* **34**, 2108830 (2022).
- [31] H. Yoo and C.-H. Kim, Multi-valued logic system: new opportunities from emerging materials and devices, *J. Mater. Chem. C* **9**, 4092 (2021).
- [32] S. L. Hurst, Multiple-valued logic—its status and its future, *IEEE Trans. Comput.* **C-33**, 1160 (1984).
- [33] Z. T. Sandhie, J. A. Patel, F. U. Ahmed, and M. H. Chowdhury, Investigation of multiple-valued logic technologies for beyond-binary era, *ACM Comput. Surv.* **54**, 30 (2021).

- [34] J. Jena, R. Stinshoff, R. Saha, A. K. Srivastava, T. Ma, H. Deniz, P. Werner, C. Felser, and S. S. P. Parkin, Observation of magnetic antiskyrmions in the low magnetization ferrimagnet $\text{Mn}_2\text{Rh}_{0.95}\text{Ir}_{0.05}\text{Sn}$, *Nano Lett.* **20**, 59 (2020).
- [35] M. J. Donahue and D. G. Porter, OOMMF User's Guide, version 1.0, Interag. Rep. NISTIR 6376, National Institute of Standards and Technology, Gaithersburg, MD (1999).
- [36] M. Beg, M. Lang, and H. Fangohr, Ubermag: Towards more effective micromagnetic workflows, *IEEE Trans. Magn.* **58**, 1 (2022).
- [37] See Sec. II of Supplemental Material at [url will be inserted by publisher] for micromagnetic simulations details.
- [38] See Sec. IV of Supplemental Material at [url will be inserted by publisher] for detailed discussion on the shape of AABs.
- [39] See Sec. III of Supplemental Material at [url will be inserted by publisher] for detailed comparison of vortex and antivortex energies for this DMI.
- [40] Note that this is not the case for symmetric bimerons [16], whose DMI is given by $D(\mathbf{e}_y \cdot \mathbf{m} \times \partial_x \mathbf{m} + \mathbf{e}_z \cdot \mathbf{m} \times \partial_y \mathbf{m})$ and the vectors are depicted in Fig. 1(e) by red arrows. Since this DMI is antisymmetric under the same mirror transformation, the symmetric bimerons favor a single topological charge value.
- [41] S. Zhang, A. A. Baker, S. Komineas, and T. Hesjedal, Topological computation based on direct magnetic logic communication, *Sci. Rep.* **5**, 15773 (2015).
- [42] J. Xia, X. Zhang, X. Liu, Y. Zhou, and M. Ezawa, Qubits based on merons in magnetic nanodisks, *Commun. Mater.* **3**, 88 (2022).
- [43] A. A. Belavin and A. M. Polyakov, Metastable states of two-dimensional isotropic ferromagnets, *JETP Lett.* **22**, 503 (1975).
- [44] O. A. Tretiakov and O. Tchernyshyov, Vortices in thin ferromagnetic films and the skyrmion number, *Phys. Rev. B* **75**, 012408 (2007).
- [45] D. Bachmann, M. Lianeris, and S. Komineas, Meron configurations in easy-plane chiral magnets, *Phys. Rev. B* **108**, 014402 (2023).
- [46] Z. Li and S. Zhang, Domain-wall dynamics and spin-wave excitations with spin-transfer torques, *Phys. Rev. Lett.* **92**, 207203 (2004).
- [47] A. Thiaville, Y. Nakatani, J. Miltat, and Y. Suzuki, Micromagnetic understanding of current-driven domain wall motion in patterned nanowires, *EPL* **69**, 990 (2005).
- [48] See Supplementary Movies 1 and 2 at [url will be inserted by publisher] for AAB dynamics with $u_x > 0$.
- [49] The potential structure is similar to interatomic potentials, such as Lennard-Jones potential.
- [50] See Supplementary Movies 3 and 4 at [url will be inserted by publisher] for AAB dynamics with $u_x < 0$.
- [51] A. A. Thiele, Steady-state motion of magnetic domains, *Phys. Rev. Lett.* **30**, 230 (1973).
- [52] O. A. Tretiakov, D. Clarke, G.-W. Chern, Y. B. Bazaliy, and O. Tchernyshyov, Dynamics of domain walls in magnetic nanostrips, *Phys. Rev. Lett.* **100**, 127204 (2008).
- [53] D. J. Clarke, O. A. Tretiakov, G.-W. Chern, Y. B. Bazaliy, and O. Tchernyshyov, Dynamics of a vortex domain wall in a magnetic nanostrip: Application of the collective-coordinate approach, *Phys. Rev. B* **78**, 134412 (2008).
- [54] See Supplementary material at [url will be inserted by publisher] for a detailed discussion on the off-diagonal component of the dissipative tensor.
- [55] Note that this consideration neglects the interaction between the merons and as a result fails to capture some details, such as saturation in the size when the texture shrinks and the difference in the Hall velocities, see Fig. 4 (a) and (b). Therefore, a more detailed theory, which includes the effect of interactions, would be required to describe this dynamics fully.
- [56] See Supplementary Movies 5 and 6 at [url will be inserted by publisher] for AAB collisions with $u_y > 0$ and $u_y < 0$, respectively.
- [57] See Supplementary Movie 7 at [url will be inserted by publisher] for behavior in the small current regime.
- [58] See Supplementary Movies 8 and 9 at [url will be inserted by publisher] for AAB collisions with $u_x > 0$ and $u_x < 0$, respectively.
- [59] K. Ohara, X. Zhang, Y. Chen, S. Kato, J. Xia, M. Ezawa, O. A. Tretiakov, Z. Hou, Y. Zhou, G. Zhao, J. Yang, and X. Liu, Reversible transformation between isolated skyrmions and bimerons, *Nano Lett.* **22**, 8559 (2022).
- [60] N. Mukai and A. O. Leonov, "Polymerization" of bimerons in quasi-two-dimensional chiral magnets with easy-plane anisotropy, *Nanomater.* **14**, 504 (2024).
- [61] P. Babu, H. P. Perumal, S. Sankaran Kunnath, and J. Sinha, Tunable creation and annihilation of magnetic bimerons in square-shaped submicron dot, *ACS Appl. Electron. Mater.* **6**, 221 (2024).
- [62] X. Yu, N. Kanazawa, X. Zhang, Y. Takahashi, K. V. Iakoubovskii, K. Nakajima, T. Tanigaki, M. Mochizuki, and Y. Tokura, Spontaneous vortex-antivortex pairs and their topological transitions in a chiral-lattice magnet, *Adv. Mater.* **36**, 2306441 (2024).